

A measure of individual role in collective dynamics

Konstantin Klemm,^{1,2} M. Ángeles Serrano,³ Víctor M. Eguíluz,² and Maxi San Miguel²

¹*Bioinformatics, Institute for Computer Science,*

Leipzig University, Härtelstrasse 16-18, 04107 Leipzig, Germany

²*Instituto de Física Interdisciplinar y Sistemas Complejos IFISC (CSIC-UIB),*

Campus Universitat Illes Balears, E07122 Palma de Mallorca, Spain

³*Departament de Química Física, Universitat de Barcelona, Martí i Franquès 1, 08028 Barcelona, Spain*

(Dated: July 21, 2021)

Identifying key players in collective dynamics remains a challenge in several research fields, from the efficient dissemination of ideas to drug target discovery in biomedical problems. The difficulty lies at several levels: how to single out the role of individual elements in such intermingled systems, or which is the best way to quantify their importance. Centrality measures describe a node's importance by its position in a network. The key issue obviated is that the contribution of a node to the collective behavior is not uniquely determined by the structure of the system but it is a result of the interplay between dynamics and network structure. We show that *dynamical influence* measures explicitly how strongly a node's dynamical state affects collective behavior. For critical spreading, dynamical influence targets nodes according to their spreading capabilities. For diffusive processes it quantifies how efficiently real systems may be controlled by manipulating a single node.

Complex networks are a groundbreaking concept that is helping to understand the behavior of many chemical, biological, social and technical systems [1, 2]. Network representations are particularly suitable for systems where heterogeneity dominates and are crucial for dynamics [3], where a few nodes are usually considered as the most important. Oftentimes, node importance is correlated with centrality measures, local [4, 5] or global [6], which usually do not explicitly account for the dynamics as they are generally based on a purely topological perspective. However, dynamics is fundamental in assessing the impact of individual elements in global performance and in controllability problems [7]. Here, we show that *dynamical influence* is a centrality measure able to quantify how strongly a node's dynamical state affects the collective behavior of a system, taking explicitly into account the interplay between structure and dynamics in complex networks. We prove that it applies equally well to a variety of families of dynamical models, from spreading phenomena at the critical point to diffusive processes and to continuous-time dynamical systems such as the Kuramoto model and the Rössler chaotic dynamics.

Classical centrality measures in complex networks – like the degree or number of neighbors a node interacts with [4, 5], betweenness centrality [8] counting the number of shortest paths through a certain node, eigenvector centrality [9] based on the idea that relations with more influential neighbors confer greater importance, or the k -shell decomposition [10] that correlates with the outcome of supercritical spreading originating in specific nodes [11–13] – rely only on topology, even if an underlying process can be indirectly associated in some cases. In contrast, the impact of individual elements in the global performance of the system inevitably depends on the specificities of the dynamics. Targeting individuals for vaccination strategies in epidemic processes is not the

same as selecting electrical stimulation sites in the brain in order to suppress epileptic seizures. In this respect, a Laplacian-based centrality measure [14–16], closely related to PageRank [17], has been proposed recently to assess the importance of complex network nodes in specific dynamical models.

In this work, we provide a general and rigorous framework where dynamical influence is defined as a centrality measure both on directed and on undirected complex networks and applies to a variety of families of dynamical models, including epidemic spreading models like the susceptible-infected-removed (SIR), the susceptible-infected-susceptible (SIS), and the contact process, the Ising model, and diffusive processes like the voter model or phase coupled oscillators. In all cases, dynamical influence is calculated as the leading left eigenvector of a characteristic matrix that encodes the interplay between topology and dynamics.

Results

Defining dynamical influence

We focus on systems of N time-dependent real variables $x = (x_1, \dots, x_N)$ with coupled linear dynamics specified by a $N \times N$ real matrix M

$$\dot{x} = Mx. \quad (1)$$

A first classification of the dynamics is obtained by considering the largest eigenvalue μ_{max} of M . For $\mu_{max} < 0$, $x(t)$ converges to a null vector that represents a stable fixed point solution; for $\mu_{max} > 0$, indefinite growth from almost all initial conditions is observed. Suppose that M is such that a non-degenerate $\mu_{max} = 0$ exists. Then, the

scalar product $\phi_c = c \cdot x$ is a conserved quantity, where c is the left eigenvector of M for μ_{max} ,

$$\frac{d\phi_c}{dt} = c \cdot \dot{x}(t) = [cM] \cdot x(t) = 0. \quad (2)$$

The existence of the conserved quantity allows to calculate the final state in terms of the initial condition $x(0)$ as

$$x(\infty) := \lim_{t \rightarrow \infty} x(t) = \frac{c \cdot x(0)}{c \cdot e} e, \quad (3)$$

where e is a right eigenvector of M for μ_{max} . This equation implies that the projection of $x(0)$ on c is all the system remembers at large times about the initial condition $x(0)$. The coefficient c_i quantifies the extent to which the initial condition at node i affects the final state. Therefore, we call c_i the *dynamical influence* (DI) of element i on the dynamics under equation (1).

One advantage of DI is that it is easily calculated without expensive numerical simulations. In fact, a simple way to calculate c furthers the understanding why this object quantifies the role of nodes in spreading dynamics. The power method (also called power iteration) [18] approximates c by applying higher and higher powers of M to a uniform vector $w^{(0)} = (1, 1, \dots, 1)$. For general exponent $l \in \mathbb{N}$, the i -th entry $w_i^{(l)}$ of

$$w^{(l)} = (1, \dots, 1)M^l \quad (4)$$

is the number of all possible walks of length l departing from node i or, in other words, the number of ways an item can spread for l steps when originating at node i . At the first iteration this yields

$$w^{(1)} = (1, \dots, 1)M = (d_1, d_2, \dots, d_n) \quad (5)$$

where d_i is the sum over the i -th row of M . When M is the adjacency matrix of a network, then $w_i^{(1)} = d_i$ is the (out-)degree, the number of (outgoing) connections of node i . For exponent 2, the i -th entry $w_i^{(2)}$ is the sum of the (out-)degrees of all neighbors of i . This is the same as the number of possibilities (walks) to depart from node i following two links. Now in the limit $l \rightarrow \infty$, the direction of the eigenvector c is approached by

$$\lim_{l \rightarrow \infty} \frac{w^{(l)}}{\|w^{(l)}\|} = \frac{c}{\|c\|} \quad (6)$$

when the largest eigenvalue of M is non-degenerate and larger in magnitude than the other eigenvalues. Hence, the dynamic influence c_i of element i is its ability to serve as the origin of many arbitrarily long walks on the network.

Epidemic spreading

Let us first apply these insights to critical phenomena like spreading processes [24]. In the SIR model [25–27], each node is either susceptible, infected or removed.

An infected node i transfers the epidemic along each of its outgoing arcs independently with probability β ; node i itself relaxes to the removed state at unit rate. We study small perturbations to the stationary state with all nodes susceptible and approximate the dynamics by the linearization

$$\dot{x} = -x + \beta A^T x. \quad (7)$$

Here $x_j(t)$ is the probability of node j to be infected at time t . The first term is the relaxation from the infected

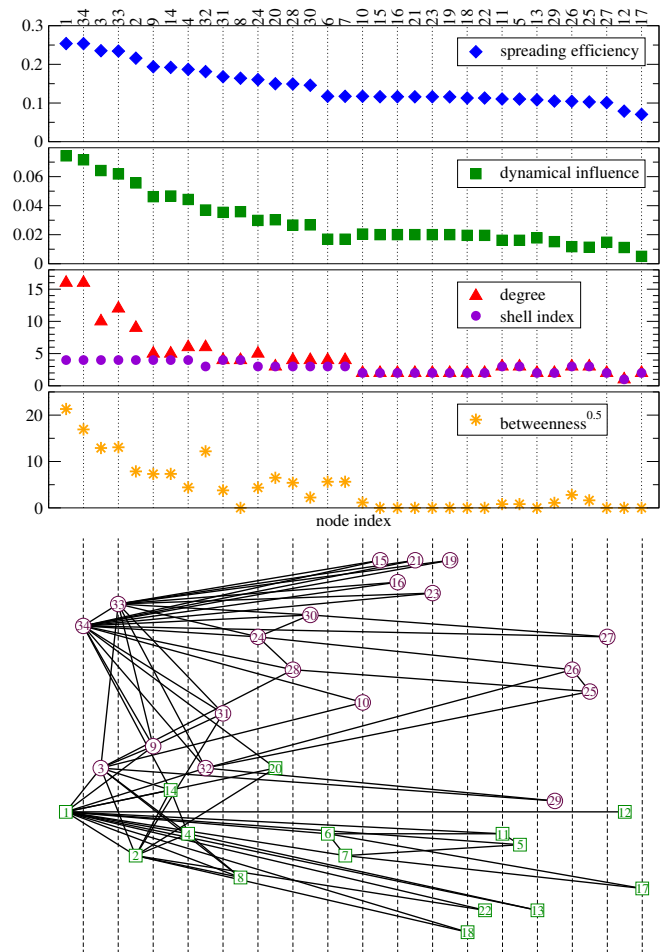


FIG. 1: SIR spreading efficiency compared to centrality measures in a social network. The network of Zachary’s karate club [19] has 77 edges connecting 34 nodes, here ordered according to decreasing spreading efficiency. A monotonic decay of a centrality measure in the diagram indicates large predictive power for spreading efficiency. The rank order correlation of spreading efficiency is of 0.97 with dynamical influence, 0.86 with degree, 0.82 with shell index, and 0.79 with betweenness centrality. Indexing of nodes is the same as in ref. [19]. In the network drawing, circles and squares represent the primary partitioning of the node set found by Girvan and Newman [20]. Spreading efficiency has been estimated at $\beta = \beta_c = 0.15$ performing 10^6 independent runs of the SIR model per seed node. The largest eigenvalue of the network adjacency matrix is 6.65.

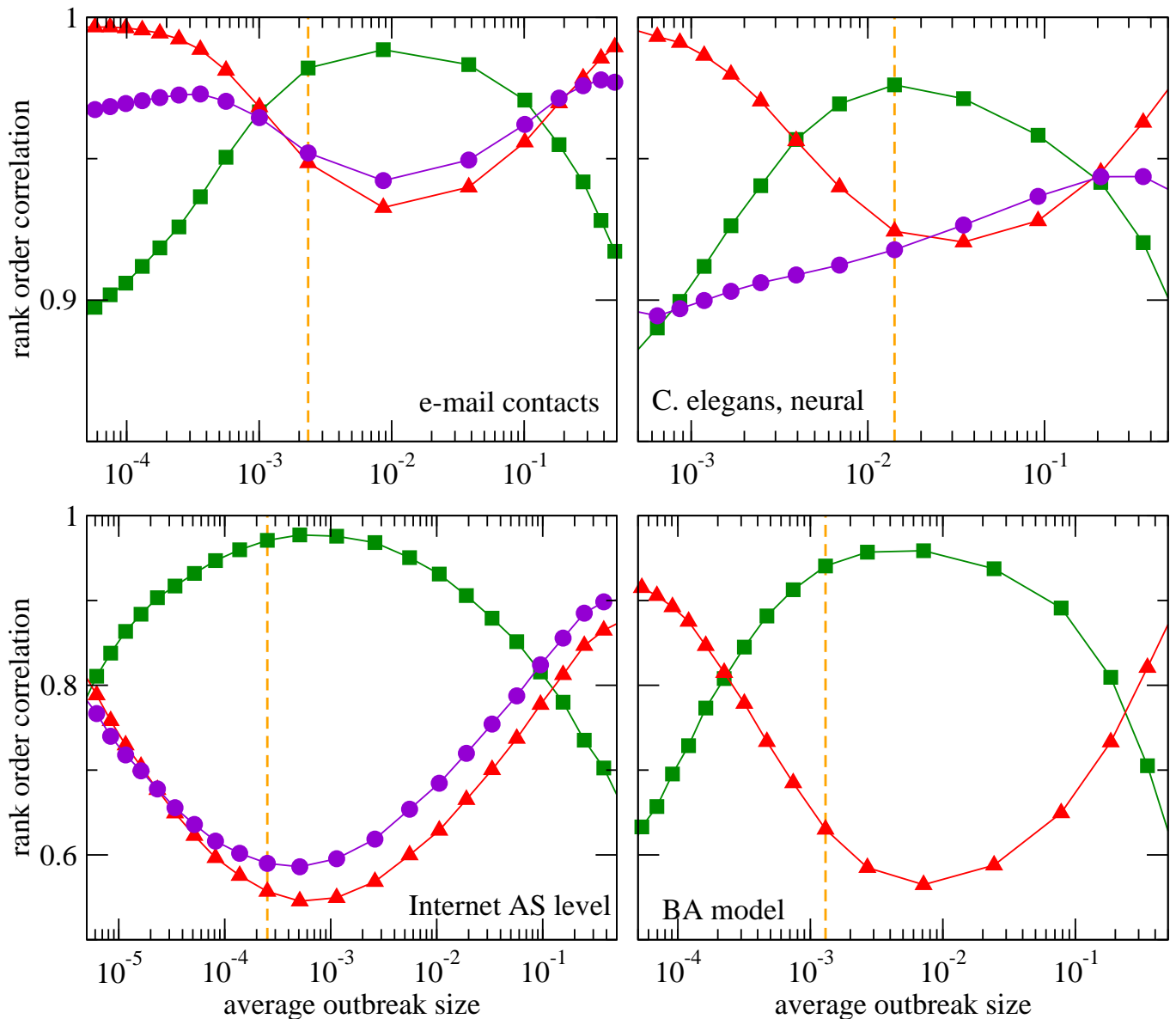


FIG. 2: Predictive power of different centrality measures for SIR spreading efficiency. Symbols are values of the rank order correlation coefficient of spreading efficiency with influence (squares), degree (triangles) and shell index (circles). The choice of the spreading parameter β controls the average outbreak size (horizontal axis), being the average number of nodes infected when choosing the seed node uniformly. The vertical dashed line indicates average outbreak size at the critical value of the spreading parameter $\beta = \beta_c$. The predictive power of betweenness centrality is below that of degree in all cases. The following networks have been used. E-mail interchanges between employees of a university [21], $\beta_c = 0.0482$; unweighted neural circuitry of the roundworm *C. elegans* [22, 23], $\beta_c = 0.0654$; snapshot of the Internet at Autonomous Systems level of Nov 08, 1997, see <http://moat.nlanr.net>, $\beta_c = 0.0315$; a realization of the Barabási-Albert (BA) model of scale-free networks [4] with 1000 nodes and $m = 2$ edges added per node, $\beta_c = 0.0945$. Other realizations of the BA model yield qualitatively the same result. For the BA model, shell index is not a predictor because its value $k_i = m$ is the same for all nodes. For the neural network, being directed, out-degree instead of degree is used as a predictor and for calculating the shell index.

to the removed state at unit rate. The second term quantifies the transmission of the epidemic where the network enters by the transpose of its adjacency matrix A .

Equation (7) can be rewritten as equation (1) with $M = \beta A^T - I$, and I being the identity matrix. Matrix M has largest eigenvalue $\mu_{max} = 0$ when the spreading

probability β is the inverse of the largest eigenvalue of A , that is $\beta = \beta_c = 1/\alpha_{max}$. We take again c as a left eigenvector of M at $\mu_{max} = 0$ or, equivalently, a right eigenvector for maximum eigenvalue α_{max} of A . Then the expected outbreak size from an initial infection described by the probability vector $x(0)$ is proportional to $c \cdot x(0)$.

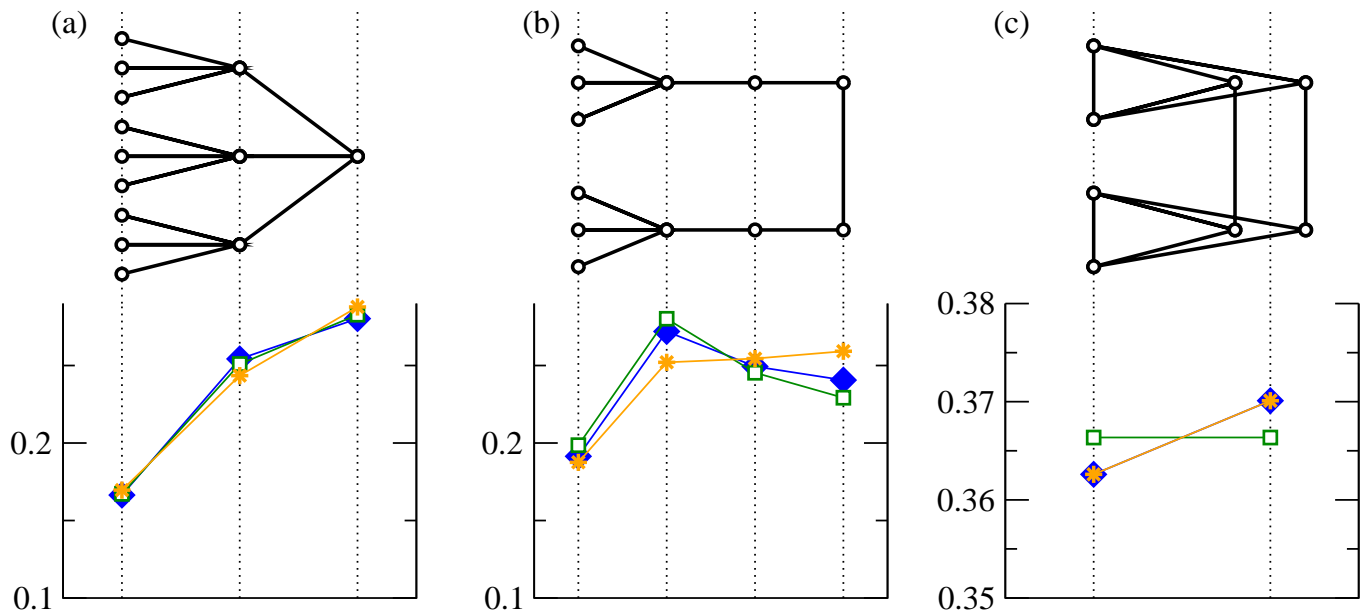


FIG. 3: Comparison between spreading efficiency (diamonds), dynamical influence (squares) and betweenness centrality (stars) in small networks. In panel (a), the ranking of nodes with respect to spreading efficiency is rendered both by dynamical influence and betweenness. Note that the most efficient spreader is not a node with maximum degree but the node on the right connected to those maximum degree nodes. In the case of panel (b), the strongest spreaders are the nodes of maximum degree 3. However, the degree does not uniquely reveal the second strongest spreaders. Dynamical influence renders the full ranking of spreading efficiency. In panel (c), nodes are indistinguishable both by degree and dynamical influence. The small differences in spreading efficiency—note the scale on the axis—on this regular graph are rendered correctly by the betweenness centrality. The shell index is not usable as a node discriminator here. It takes value 1 on each node in panels (a) and (b) and the value 3 in panel (c). Spreading efficiency is calculated at the critical value $\beta = \beta_c$ for each network, being 0.408 for (a), 0.463 for (b), and 0.333 for (c). For easier comparison, values of dynamical influence and betweenness centrality have been rescaled and shifted such that their mean and standard deviation are identical to that of the spreading efficiency in each network.

Now we ask how well c may forecast the actual SIR spreading dynamics, measured as the *spreading efficiency* (details in Methods) of node i that we define as the expected fraction of nodes reached by an epidemic outbreak initiated with node i infected (*seed node*), all others susceptible. Figure 1 shows that c_i is a good predictor of SIR spreading efficiency at critical parameter value $\beta = \beta_c$ in a small social network. Dynamical influence c_i outperforms the predictions made by degree, shell index and betweenness centrality. Predictive power is quantified by the rank order correlation (see Methods).

Figure 2 shows the predictive power of dynamical influence for spreading efficiency as a function of the infection probability in larger real-world networks and the Barabasi-Albert model. The results are as anticipated by the theory. Dynamical influence is a good predictor of spreading efficiency in the critical regime where $\beta/\beta_c \approx 1$. Predictions by dynamical influence outperform those by other quantities that are supposed to provide information about expected outbreak size in a broad interval of infection probabilities. This still holds for values of β that lead to average outbreak sizes of up to 10% of all nodes in the network, as indicated by the vertical dashed lines in Figure 2.

The approximation $w^{(l)}$ for *finite* length l in Eq. (4) is

useful as a predictor of spreading efficiency as well. Even when the interaction network is not completely available, local information counting the number of walks of length $l = 2$ or $l = 3$ emanating from a node is enough to estimate dynamical influence. Figure S1 in the Supplementary Information shows that the count of these short walks yields a prediction of spreading efficiency in the critical regime that is as good as dynamical influence itself. The predictive power of these walk counts, too, reaches a maximum in the critical regime.

For infection probabilities β far above or below the critical value β_c , however, the degree d_i of a node i is a better predictor of spreading efficiency. In the subcritical regime, spreading is sparse and typically confined to the neighborhood of the seed node i , while in the supercritical regime, the epidemics rarely fails to spread to the whole system. In the critical regime in-between these extremes, infectious seeds are perturbations that trigger relaxation dynamics at all scales. This is reflected in a dynamics dominated by a marginal linear mode and a variety of possible final states. Dynamical predictions at criticality require then a global view of the network structure (and the final state is determined by the conservation law associated with the leading eigenvector c -removed). The scale-free distribution of epidemic outbreaks in real pop-

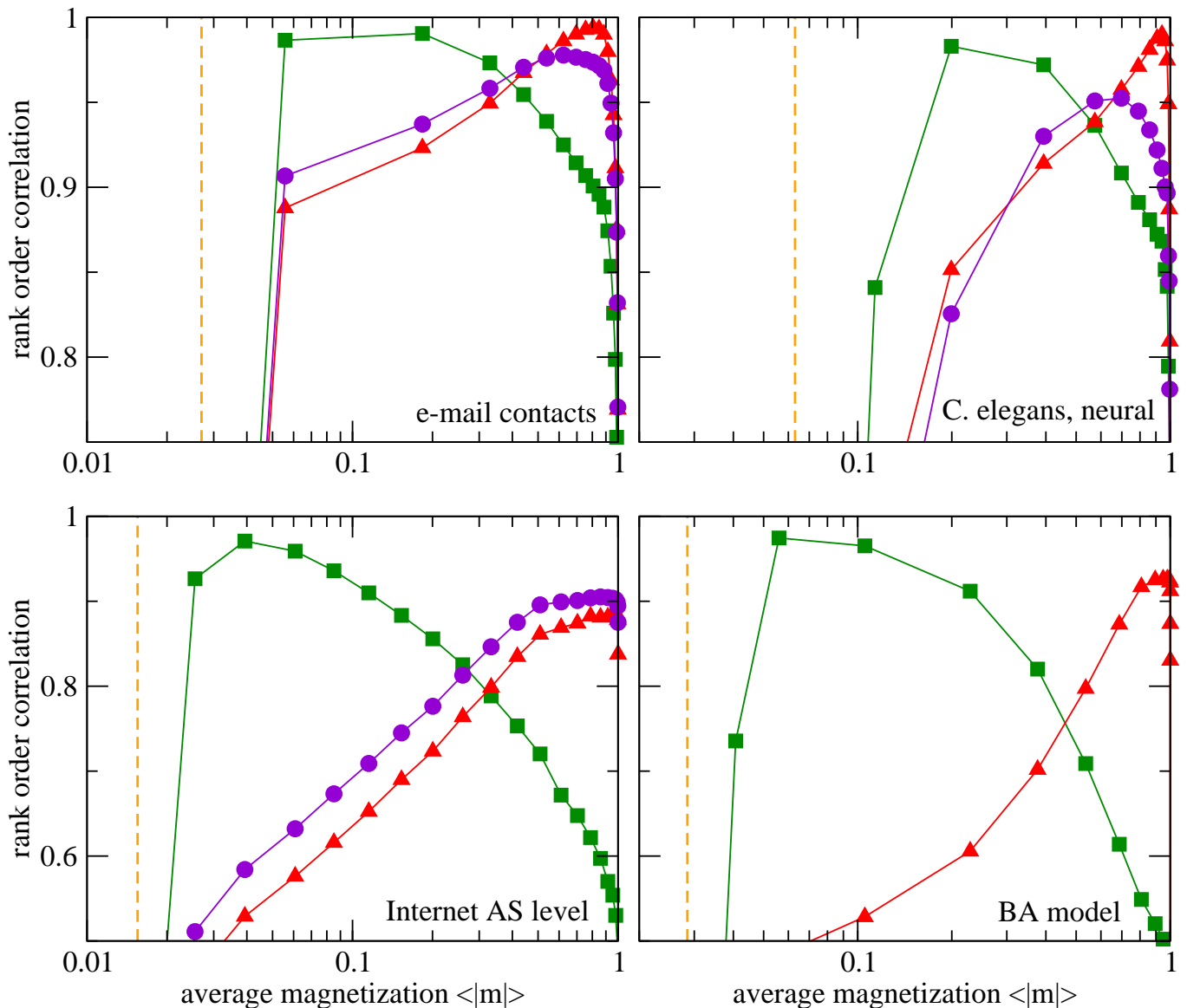


FIG. 4: Predictive power of different centrality measures for Ising spreading efficiency at time lag $\tau = 10$ as a function of average absolute magnetization $\langle |m| \rangle$. Symbols are values of the rank order correlation coefficient of spreading efficiency with influence (squares), degree (triangles) and shell index (circles). The vertical dashed lines indicate the value of $\langle |m| \rangle$ at the critical parameter value $\beta = \beta_c$. Details on networks and the values of β_c are given in the caption of Figure 2.

ulations [28, 29] is a sign of criticality and suggests that this regime is most relevant in practice.

In order to check the robustness of the results we consider two modifications of the epidemic spreading dynamics. First, we study the SIR model with a stochastic rather than deterministic transition from the infected to the removed state. Specifically, the transition occurs with a probability μ independently for each infected node at each time step. Thus the time spent in the infected state (recovery time) has a geometric distribution with mean μ^{-1} . This modification does not qualitatively change the results of Figure 2 up to rescaling of β with μ . In fact, the curves of predictive power for different values

of μ collapse when plotted as a function of the average outbreak size, see Figure S2. Second, prediction by dynamical influence may also be applied to the SIS model (see Materials and methods) yielding very similar results (Supplementary Information, Figure S3). The contact process [30] can also be considered, with A replaced by the stochastic adjacency matrix, the adjacency matrix after normalization such that each row sums up to 1.

To facilitate intuitive understanding of the predictive role of centrality measures in spreading dynamics, let us consider small networks. In each of the three cases in Fig. 3, a different subset of the measures yields the correct ranking by spreading efficiency at the critical point.

The most efficient spreader is not necessarily the node with the largest degree. Being adjacent to several nodes with large degree may lead to large spreading efficiency despite a smaller degree, cf. panel (a). This second order effect is reflected by dynamical influence. When all degrees are equal as in panel (c), also dynamical influence and shell index are homogeneous. In this case, betweenness centrality captures the subtle effect of nodes having different positions in the network. We speculate that centrality measures based on unconstrained walks and shortest paths can do best in predicting spreading efficiency at the critical point. Then, a suitable combination of dynamical influence with betweenness depending on network topology might be close to the optimal predictor.

Nodes with large shell index are contained in highly connected neighborhoods that facilitate spreading. In many cases, the shell index may serve as a satisfactory predictor of spreading efficiency [13]. Here, however, we find situations where its use for prediction is limited due to the degeneracy of the values shell index assumes. It has a constant value m across nodes of each network that can be built up by iterative attachment of a node with exactly m edges. This includes all trees ($m = 1$) and networks from growth models such as the one by Barabasi and Albert [4]. A significant lack of resolution is also observed in real-world networks. Shell index assumes only few (≈ 10) discrete values, cf. Figure S4 in Supplementary Information. On the Internet graph, the same maximum shell index value is observed for the strongest spreader as well as nodes with spreading efficiency a factor of five below. Thus, even though the overall correlation between spreading efficiency and shell index is positive, lack of resolution limits the predictive power. Such limitations have been identified also in an empirical study of epidemic spreading in a social group [31], in a detailed comparison between SIR and SIS models [32] and in dynamics of rumour propagation [33].

We remark that the most efficient spreaders are not necessarily the same as those targeted by efficient vaccination strategies in order to contain epidemics. At the network level, the aim of vaccination is to increase the epidemic threshold β in order to render the spreading dynamics subcritical. The set of nodes by whose removal this shift of threshold is achieved [34] is different in general from the set of nodes with the largest dynamical influence. The Supplementary Information provides further results (Figure S5) and a brief discussion of vaccination.

Ising model

The Ising model is a paradigmatic binary state model of critical phenomena. The Ising model [35, 36] on a network [37] describes the dynamics of N coupled spins $s_i \in \{-1, +1\}$ placed on the nodes. The zero temperature ($T=0$) version of the Ising model implements a ma-

ajority rule for state updating. This is the same dynamics considered in threshold models of collective behavior for a 50% value of the threshold [38, 39], and its dynamics is also related to Schelling's model of urban segregation [40, 41]; the finite temperature version has been considered in the context of strategic interactions [42]. Finite temperature effects (noise), as considered here, are essential to escape from frozen configurations and to establish the robustness of transitions found in Ising-like models [43]. Also in the theory of neural computation, Ising-like systems play an essential role [44].

In the context of the Ising model, we define spreading efficiency of node i as the correlation between two measurements: the state of node i at time t and the magnetization (see Methods) of the whole system at a later time, formally

$$f_i(\beta) = \langle s_i(t)m(t + \tau N) \rangle. \quad (8)$$

The parameter τ measures the time lag between the two measurements. Figure 4 shows to which extent the ranking of nodes by Ising spreading efficiency is correlated with the ranking by various centrality measures. At the transition between order and disorder, Ising spreading efficiency has larger correlation with dynamical influence than with the other centrality measures.

Diffusive processes: the voter model

Coming back to the general framework equation (1), there is a class of dynamical processes in networks in which the property of M having a zero maximum eigenvalue appears naturally without the need of adjusting any parameter. This is the case of diffusive processes defined by equation (1) with $M = -L$ and the Laplacian matrix entries

$$L_{ij} = -K_{ij} + \delta_{ij} \sum_{k=1}^N K_{ik}. \quad (9)$$

The zero eigenvalue of L is non-degenerate under mild assumptions [45]. For these processes our general analysis of equation (1) becomes exact. A prominent example of diffusive dynamics is the voter model [46] in which node i is in a spin state $s_i \in \{-1, +1\}$. For this model, x_i stands for the ensemble average of spin i , $x_i = \langle s_i \rangle$, and K_{ij} gives the rate at which node i copies the state of node j . Different definitions of the voter model dynamics provide clear examples of how the concept of dynamical influence takes into account the interplay between topology and dynamics: For *link update* dynamics in an undirected network, an ordered pair of nodes (i, j) is chosen in each step and node i copies the state of node j . The rate matrix K becomes proportional to the transpose of the adjacency matrix A . As a consequence $c_i = 1/N$, the average magnetization $\sum_{i=1}^N c_i x_i$ is conserved, and all nodes have the same dynamical influence independently of the topological features of the network. In the

more standard *node update* voter dynamics, at each step one node i (having degree d_i) is selected at random and copies the state of one of its neighbors j , also selected at random. In this case $K_{ij} \propto A_{ji}/d_i$, so that K_{ij} is no longer a symmetric matrix, the conserved quantity is a weighted magnetization [47] and the dynamical influence of node i is proportional to its degree d_i .

For diffusive processes, the system is driven towards a homogeneous final state with $x^* := x_i(\infty) = x_j(\infty)$ for all i and j . Although x^* takes continuous values, each realization of the voter dynamics in a finite system eventually reaches a homogeneous absorbing state with either all nodes in the state $+1$ or all in the state -1 . The influence c_i of a node weights the initial state of node i in the exit probability P_+ , that is, the probability to reach the absorbing configuration $+1$: $P_+ = (\phi_c + 1)/2 = (x^* + 1)/2$. When all nodes are equivalent (e.g., link update) x^* is just the average of the initial values of the nodes, but otherwise (e.g. node update) x^* is given by a weighted average of the initial condition. The value c_i has an alternative interpretation as a stationary density of a random walk [15].

Efficient driving of complex systems

The meaning of dynamical influence also manifests itself in the practical task of driving a system efficiently. In the context of the zealot problem [49]. One considers a special directed network in which a given node (the zealot) does not copy the state of any of its neighbors. The question is the efficiency of the zealot in driving all other nodes to the zealot state. To show the broad applicability of the dynamical influence concept, we address this question of driving efficiency considering the problem of phase-coupled oscillators described by the Kuramoto model [50]. Assuming all oscillators have the same intrinsic frequency ω (without losing generality, we choose $\omega = 0$), the phase variable x_i of oscillator i advances as

$$\dot{x}_i = \omega + \sum_{j=1}^N K_{ij} \sin(x_j - x_i). \quad (10)$$

with a matrix K of non-negative coupling strengths. Around the synchronized state, phase differences are small. By approximating each sin-term with its argument, a linear homogeneous system as in equation (1) is recovered.

We study a scenario with initially all oscillators i in phase $x_i(0) = 0$. An additional node a with constant phase $x_a = \pi/2$ is added to the system and linked through an additional edge to a chosen node i . We measure the time T_i the system takes to reach the new homogeneous state with $s_i = \pi/2$ for all nodes i . The dynamical evolution of these systems is illustrated by studying the motif in the inset of Fig. 5a. The global phase $\psi(t)$ converges faster to the external forcing when

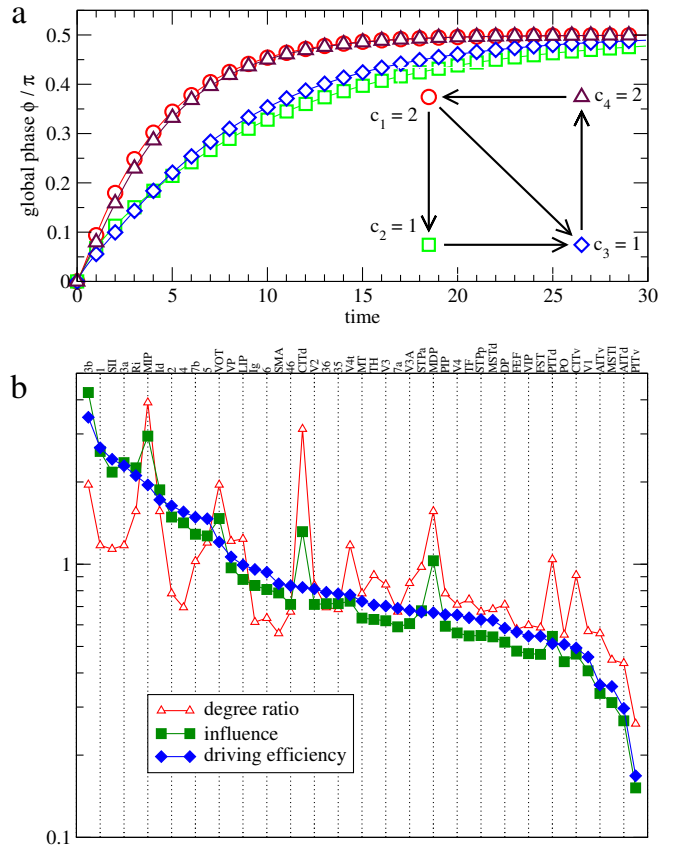


FIG. 5: Dynamical influence and driving in a system of phase-coupled oscillators. **a** Adaptation of the *global* phase of the four-node system in the inset when driving is applied to one of the oscillator nodes (an additional oscillator coupled to the red circle node with fixed phase $\pi/2$). Adaptation is quick when driving at nodes 1 (o) and 4 (Δ), having high influence, and slow when driving at one of the other two nodes, having low influence. **b**, Driving efficiency (filled diamonds) and dynamical influence (shaded squares) for a system of phase oscillators coupled as the network of regions in the macaque cortex [48]. Driving efficiency of node i is measured as the time required to resynchronize with an additional input signal applied to a given node i . We say that the system has resynchronized when the global phase reaches $\psi(t) \geq (1 - \epsilon)x_a$ with a tolerance $\epsilon = 10^{-2}$, where the global phase $\psi(t)$ is computed as the argument of the global order parameter $z(t) = r \exp[i\psi(t)] = \sum_{i=1}^N \exp[is_i(t)]$. For comparison, the degree ratio $k_{\text{out}}/k_{\text{in}}$ of each node is also shown (open triangles). Since this is not an uncorrelated network, node influence deviates significantly from degree ratio. Each plotted quantity is rescaled by a factor to obtain an average value of 1. The empirical network serves as a testbed for prediction of driving efficiency. We do not aim to mimic real dynamics of the cortex.

the driving is applied to the nodes with higher influence, and the convergence of the different nodes depends on their relative network position in relation to the driver. In Fig. 5(b), we show the results on a directed network of phase oscillators connected as the network of regions in the macaque cortex [48]. Dynamical influence has ex-

tremely high predictive power. The rank order correlation of driving efficiency with dynamical influence is 0.97, while 0.66 with degree ratio, -0.14 with shell index and -0.09 with betweenness. Similar results are obtained on randomly grown directed networks and for coupled chaotic oscillators, see Figures S6 and S7 in Supplementary Information. These findings clearly show that dynamical influence is an excellent proxy to identify better targets for controlling global behavior, even in strongly non-linear dynamical systems.

Discussion

Dynamical influence is a centrality measure applicable to a wide range of dynamical processes on complex networks that takes into account the interplay between topology and dynamics. While the motivation and rigorous analysis of dynamical influence employ the context of linear systems, its practical use for understanding and controlling networked dynamics extends to several inherently non-linear systems.

We have demonstrated that dynamical influence is applicable to stochastic equilibrium (Ising model) and non-equilibrium systems (epidemic and voter models) as well as deterministic state-continuous systems such as the Kuramoto model and the chaotic Roessler attractor. For critical epidemic spreading and the Ising model, dynamical influence is a good predictor of spreading capabilities. In the context of chaotic Boolean dynamics [51], a similar spectral centrality is highly correlated with a node's impact on the attractor reached [52]. For diffusion, dynamical influence quantifies the impact of the dynamical states of single nodes on the asymptotic homogeneous state. Beyond that, it proves to be a high-quality proxy for driving efficiency, uncovering which are the best target nodes in real networks to be forced in order to drive the system towards specific states. In a broader context, the identification of these targets has fundamental implications and practical applications on strategies with an interest in controlling collective behavior, from social influence to biomedical responses.

Methods

Epidemic models

We simulate the *SIR model* of epidemic spreading in the time-discrete version. Transitions between the three states (S,I,R) are as follows. If node i is in the S (susceptible) state and has ν infected (I) neighbors at time t , then node i remains susceptible with probability $(1-\beta)^\nu$, otherwise i is infected at time $t+1$. If node i is in the infected state at time t then i is in the R (removed) state at time $t+1$. In the *SIS model*, at difference with SIR, a node infected at time t is susceptible again at time $t+1$. The probability of being removed in the *SIR model* does

not enter in the linearized equation (7) because it appears only in a second order term in the equation for x . Therefore equation (7) gives the same linear description for the *SIR* and *SIS* models.

The system is in an absorbing configuration if none of the nodes is infected. For both models, outbreak size is the number of nodes having been infected at least once before reaching an absorbing configuration. The spreading efficiency of node i is the average outbreak size when initiating the dynamics with node i infected and all others susceptible.

Ising model

The spin values $s_i \in \{-1, +1\}$ are updated asynchronously as follows. At each time step t , a node $i \in \{1, \dots, N\}$ is drawn uniformly. The field

$$h_i(t) = \sum_{j=1}^N K_{ij} s_j(t) \quad (11)$$

is calculated. The state of node i is flipped with probability

$$\min\{\exp[-\beta s_i(t) h_i(t)], 1\}. \quad (12)$$

Flipping the state of node i means $s_i(t+1) = -s_i(t)$. Otherwise the state of node i remains unchanged. All other nodes $j \neq i$ retain their state, $s_j(t+1) = s_j(t)$.

The parameter β (inverse temperature) controls the order in the system. For large β (small temperature), spins tend to align and there is long-range order seen as large clusters of nodes sharing the same spin value. For small β (high temperature), long-range order is absent. The magnetization

$$m(t) = N^{-1} \sum_{i=1}^N s_i(t). \quad (13)$$

is used to quantify the order of the system. Disordered systems have $\langle m \rangle \approx 0$, while a finite positive value is obtained in ordered systems.

Rank order correlation

For a vector $x \in \mathbb{R}^n$, the rank of component i is given by

$$r_i(x) = 1 + |\{j \neq i | x_j > x_i\}| + \frac{1}{2} |\{j \neq i | x_j = x_i\}| \quad (14)$$

The rank order correlation coefficient $\rho(x, y)$ between two such vectors x and y is the Pearson correlation coefficient between the rank vectors $r(x)$ and $r(y)$. Thus $\rho(x, y)$ takes values in $[-1, 1]$ with $\rho(x, y) = +1$ (-1) if and only if x and y are in a strictly increasing (decreasing) relation.

Degree and degree ratio

The degree d_i of node i is the number of nodes i is connected to. In directed networks, in- and out-degree d_i^{in} and d_i^{out} are distinguished. For the matrix averag-

ing over all adjacency matrices of networks with fixed node degrees, $c_i = d_i$ is a left eigenvector for the largest eigenvalue. Likewise, the degree ratios $d_i^{\text{out}}/d_i^{\text{in}}$ form a left eigenvector of the Laplacian matrix averaging over all networks with given node degrees [53, 54].

-
- [1] S. N. Dorogovtsev and J. F. F. Mendes, *Evolution of networks: From biological nets to the Internet and WWW* (Oxford University Press, Oxford, 2003).
- [2] R. Albert and A.-L. Barabási, *Rev. Mod. Phys.* **74**, 47 (2002).
- [3] R. Pastor-Satorras and A. Vespignani, *Physical Review Letters* **86**, 32003203 (2001).
- [4] A.-L. Barabási and R. Albert, *Science* **286**, 509 (1999).
- [5] H. Jeong, S. P. Mason, A.-L. Barabási, and Z. N. Oltvai, *Nature* **411**, 41 (2001).
- [6] S. Wuchty and P. F. Stadler, *Journal of Theoretical Biology* **223**, 45 (2003).
- [7] Y.-Y. Liu, J.-J. Slotine, and A.-L. Barabási, *Nature* **43**, 123 (2011).
- [8] L. Freeman, *Sociometry* **40**, 35 (1977).
- [9] P. Bonacich, *Journal of Mathematical Sociology* **2**, 113 (1972).
- [10] B. Bollobás, *Graph Theory and Combinatorics: Proceedings of the Cambridge Combinatorial Conference in Honor of P. Erds Vol. 35* (Academic, 1984).
- [11] S. B. Seidman, *Social Networks* **5**, 269 (1983).
- [12] S. N. Dorogovtsev, A. V. Goltsev, and J. F. F. Mendes, *Phys. Rev. Lett.* **96**, 040601 (2006).
- [13] M. Kitsak, L. K. Gallos, F. Liljeros, L. Muchnik, H. E. Stanley, and H. A. Makse, *Nature Physics* **6**, 888893 (2010).
- [14] N. Masuda, Y. Kawamura, and H. Kori, *New Journal of Physics* **11**, 113002 (2009).
- [15] N. Masuda and H. Kori, *Phys. Rev. E* **82**, 056107 (2010).
- [16] B. Golub and M. O. Jackson, *American Economic Journal: Microeconomics* **2**, 112 (2010).
- [17] S. Brin and L. Page, *Proceedings of the Seventh International World Wide Web Conference, Computer Networks and ISDN Systems* **30**, 107 (1998).
- [18] R. V. Mises and H. Pollaczek-Geiringer, *ZAMM - Journal of Applied Mathematics and Mechanics / Zeitschrift für Angewandte Mathematik und Mechanik* **9**, 58 (1929), ISSN 1521-4001.
- [19] W. W. Zachary, *Journal of Anthropological Research* **33**, 452 (1977).
- [20] M. Girvan and M. E. J. Newman, *Proceedings of the National Academy of Sciences of the USA* **99**, 7821 (2002).
- [21] R. Guimerà, L. Danon, A. Díaz-Guilera, F. Giralt, and A. Arenas, *Phys. Rev. E* **68**, 065103 (2003).
- [22] D. J. Watts and S. H. Strogatz, *Nature* **393**, 440 (1998).
- [23] J. G. White, E. Southgate, J. N. Thomson, and S. Brenner, *Philosophical Transactions of the Royal Society of London. B, Biological Sciences* **314**, 1 (1986).
- [24] S. N. Dorogovtsev, A. V. Goltsev, and J. F. F. Mendes, *Rev. Mod. Phys.* **80**, 1275 (2008).
- [25] M. J. Keeling and P. Rohani, *Modeling Infectious Diseases in Humans and Animals* (Princeton University Press, 2007).
- [26] S. Bansal, B. T. Grenfell, and L. A. Meyers, *Journal of The Royal Society Interface* **4**, 879 (2007).
- [27] T. House and M. J. Keeling, *Journal of The Royal Society Interface* (2011).
- [28] C. J. Rhodes and R. M. Anderson, *Nature* **381**, 600 (1996).
- [29] O. A. Pinto and M. A. Muñoz, *PLoS ONE* **6**, e21946 (2011).
- [30] T. E. Harris, *Ann. Probab.* **2**, 969 (1974).
- [31] N. A. Christakis and J. H. Fowler, *PLoS ONE* **5**, e12948 (2010).
- [32] C. Castellano and R. Pastor-Satorras, *ArXiv e-prints* (2011), 1105.5545.
- [33] J. Borge-Holthoefer and Y. Moreno, *ArXiv e-prints* (2011), 1112.2239.
- [34] J. G. Restrepo, E. Ott, and B. R. Hunt, *Phys. Rev. Lett.* **97**, 094102 (2006).
- [35] E. Ising, *Zeitschrift für Physik A, Hadrons and Nuclei* **31**, 253 (1925), ISSN 0939-7922.
- [36] S. G. Brush, *Rev. Mod. Phys.* **39**, 883 (1967).
- [37] S. N. Dorogovtsev, A. V. Goltsev, and J. F. F. Mendes, *Phys. Rev. E* **66**, 016104 (2002).
- [38] M. Granovetter, *American J Sociol* **83**, 14201443 (1978).
- [39] J. C. González-Avella, V. M. Eguíluz, M. Marsili, F. Vega-Redondo, and M. San Miguel, *PLoS ONE* **6**, e20207 (2011).
- [40] T. Schelling, *J. Math. Sociol.* **1**, 143 (1971).
- [41] D. Vinkovic and A. Kirman, *Proc. Natl. Acad. Sci. (USA)* **103**, 19261 (2006).
- [42] L. E. Blume, *Games and Economic Behavior* **5**, 387 (1993).
- [43] K. Klemm, V. M. Eguíluz, R. Toral, and M. San Miguel, *Physical Review E* **67**, 045101(R) (2003).
- [44] J. Hertz, A. Krogh, and R. G. Palmer, *Introduction to the Theory of Neural Computation* (Addison-Wesley, 1991).
- [45] R. Agaev and P. Chebotarev, *Linear Algebra and its Applications* **399**, 157 (2005), special Issue devoted to papers presented at the International Meeting on Matrix Analysis and Applications, Ft. Lauderdale, FL, 14-16 December 2003.
- [46] R. Holley and T. Liggett, *Annals of Probability* **3**, 643 (1975).
- [47] K. Suchecki, V. M. Eguíluz, and M. San Miguel, *Europhysics Letters* **69**, 228 (2005).
- [48] C. J. Honey, R. Kötter, M. Breakspear, and O. Sporns, *Proceedings of the National Academy of Sciences of the USA* **104**, 10240 (2007).
- [49] M. Mobilia, *Phys. Rev. Lett.* **91**, 028701 (2003).
- [50] J. A. Acebrón, L. L. Bonilla, C. J. Pérez Vicente, F. Ritort, and R. Spigler, *Reviews of Modern Physics* **77**, 137 (2005).
- [51] S. A. Kauffman, *The Origins of Order* (Oxford University Press, New York, 1993).
- [52] F. Ghanbarnejad and K. Klemm, *ArXiv e-prints* (2011), 1111.5334.

- [53] M. A. Serrano, K. Klemm, F. Vazquez, V. M. Eguíluz, and M. San Miguel, *Journal of Statistical Mechanics: Theory and Experiment* **2009**, P10024 (2009).
- [54] N. Masuda and H. Ohtsuki, *New Journal of Physics* **11**, 033012 (2009).

Acknowledgments

K.K. acknowledges financial support from VolkswagenStiftung and from European Commission NEST Pathfinder initiative on Complexity through project SYNLET (Contract 043312). M.A.S. acknowledges financial support by the Ramón y Cajal program of the Spanish Ministry of Science, MICINN Project No. BFU2010-21847-C02-02, and Generalitat de Catalunya grant No. 2009SGR1055. V.M.E. and M.S.M. acknowledge financial support from MICINN (Spain) and FEDER (EU) through projects FISICOS (FIS2007-60327) and MODASS (FIS2011-24785).

SUPPLEMENTARY MATERIAL

Epidemic spreading

We test the idea of approximating dynamical influence by applying a finite (l -th) power of the adjacency matrix to a uniform vector, cf. section *Defining dynamical influence* of the main article. The resulting quantity is $w_i^{(l)}$, the number of walks of length l departing from a node. Figure S1 shows that the number of walks of length $l \geq 2$ is a good predictor of spreading efficiency in the critical regime, even for moderate l .

Further results on epidemic spreading to support the robustness of dynamic influence as a predictor for spreading efficiency. Figure S2 compares results for the SIR model with different recovery probability μ . At each time step, an infected (I) node changes state to recovered (R) with probability μ and stays infected with probability $1 - \mu$. The case of deterministic recovery in a single step ($\mu = 1$) is the one treated in Figure 2 in the main article. In Figure S3, results for the SIS model are presented analogous to those for the SIR model, cf. Figure 2 in the main article.

Figure S4 provides the detailed relation between centrality measures (shell index, influence) and spreading efficiency at criticality for the standard SIR model ($\mu = 1$). In the network of e-mail contacts, the maximum shell index $k_{\max} = 11$ is not assumed by any of the top spreaders. In the neural network of *C. elegans*, $k_{\max} = 7$ is assumed by the 76 top spreaders out of the 274 nodes. Across these 76 nodes, spreading efficiency varies by a factor of 2.75. Likewise, the 26 top spreaders out of the 3015 autonomous systems of the Internet graph have $k_{\max} = 9$, with spreading efficiency varying by a factor of more than five across these 26 nodes. Finally, the macaque cortex network has 47 nodes in total; spreading efficiency varies by a factor of 1.96 across the 23 top spreaders belonging to the innermost shell of $k_{\max} = 8$.

Furthermore, we study a scenario of epidemic spreading with a fraction of the nodes vaccinated and thus immune. For these purposes, the vaccinated nodes and their connections are removed from the network before running the SIR dynamics. In order to test the suitability of a centrality measure for defining a vaccination strategy, the removed nodes are those ranking highest under the centrality measure. Figure S5 shows that outbreak size is reduced most when vaccinating the nodes with the largest degree or the largest betweenness centrality. Shell index and dynamical influence provide less guidance when selecting candidates for vaccination. All four centrality measures perform better than a purely random assignment of centrality values.

Why is the node set to be chosen for efficient vaccination not the same as the group of efficient spreaders at criticality? Removing central nodes is expected to drastically reduce the largest eigenvalue of the network and thereby increase the epidemic threshold. Very few node

removals may render the dynamics subcritical on the network of remaining nodes. Once in the subcritical regime, the degree is the centrality measure that best predicts spreading efficiency. Thus for vaccination, nodes are to be selected by degree rather than dynamical influence.

Driving coupled oscillators

Further simulations of the driven system of phase-coupled oscillators are performed, on randomly grown networks with (a) geometric (exponential) in- and out-degree distributions and (b) a broad (scale-free) distribution of out-degree and a geometric distribution of in-degree. The rank-order correlation between driving efficiency and several centrality measures is shown in Figure S6 as a function of network size.

Next we replace the Kuramoto oscillators by Rössler oscillators diffusively coupled by all three variables. The autonomous dynamics evolves as

$$\begin{aligned} \dot{x}_i &= -y_i - z_i & + \eta \sum_{j=1}^N K_{ij}(x_j - x_i) \\ \dot{y}_i &= x_i + 0.2y_i & + \eta \sum_{j=1}^N K_{ij}(y_j - y_i) \\ \dot{z}_i &= 0.2 + z_i(x_i - 9) & + \eta \sum_{j=1}^N K_{ij}(z_j - z_i) \end{aligned} .$$

with (x_i, y_i, z_i) the three-dimensional state vector of node i and the coupling matrix K of the network. The coupling strength is set $\eta = 10$. As the initial condition, all nodes in the network obtain the same state $x_i(0) = x^{(0)}$, $y_i(0) = y^{(0)}$, $z_i(0) = z^{(0)}$, $i \in \{1, \dots, N\}$ such that these oscillators are synchronous at the beginning. We draw $x^{(0)}$, $y^{(0)}$, $z^{(0)}$ as independent standard random numbers, i.e. from the uniform distribution on the unit interval. The driving node is initialized independently, drawing standard random numbers for all three variables. Then, as in the previous scenario with the Kuramoto oscillators, a directed coupling (also of strength η) is established from the driving node to a chosen node i . The time T_i until synchronization is measured. Synchronization is reached when for each node j the absolute difference between the driving node's state and the state of node j is below ϵ in all three variables, with $\epsilon = 10^{-4}$. If synchronization is not reached by time $t = 10^3$, $T_i = 10^3$ is assigned. The driving efficiency of node i is the inverse of the time until synchronization when the driving node feeds into node i as described. The Macaque cortex network is used for the simulations.

Predictive power of centrality measures is similar to the case of Kuramoto oscillators. Driving efficiency has a rank order correlation of 0.957 ± 0.010 with dynamical influence, 0.646 ± 0.012 with degree ratio, -0.013 ± 0.011 with shell index, and -0.072 ± 0.007 with betweenness. These estimates are obtained as mean values and standard deviations over 10 independent realizations (initial conditions). Figure S7 shows the driving efficiencies obtained in these realizations, with nodes ordered by dynamical influence.

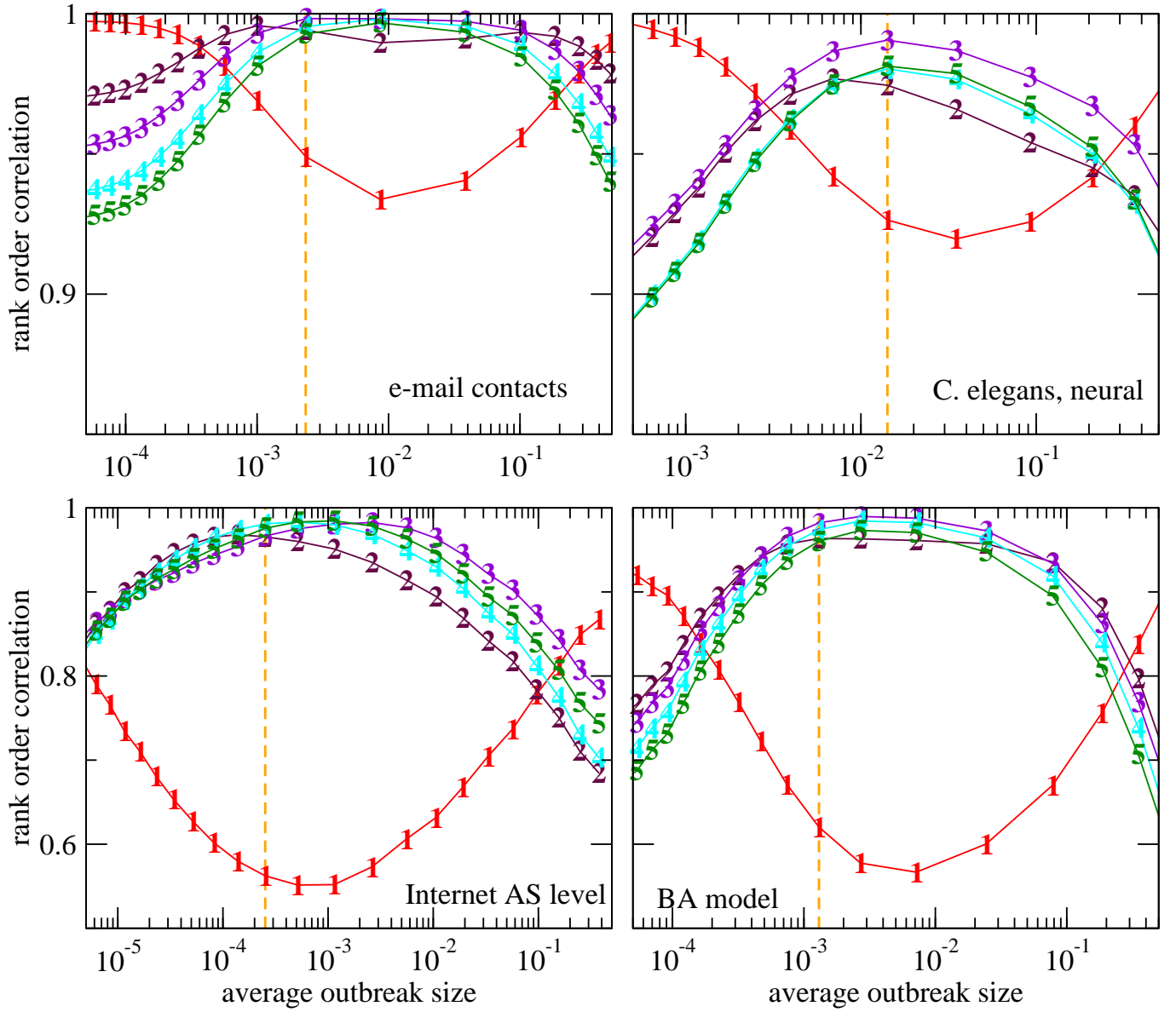


FIG. S1: Prediction of SIR spreading efficiency of a node i by the number of walks $w_i^{(l)}$ of a given length l and starting at i . Symbols indicate the value of length l . For $l = 1$, the number of walks is the (out-)degree. Further details are identical to those of Fig. 2 in the main article.

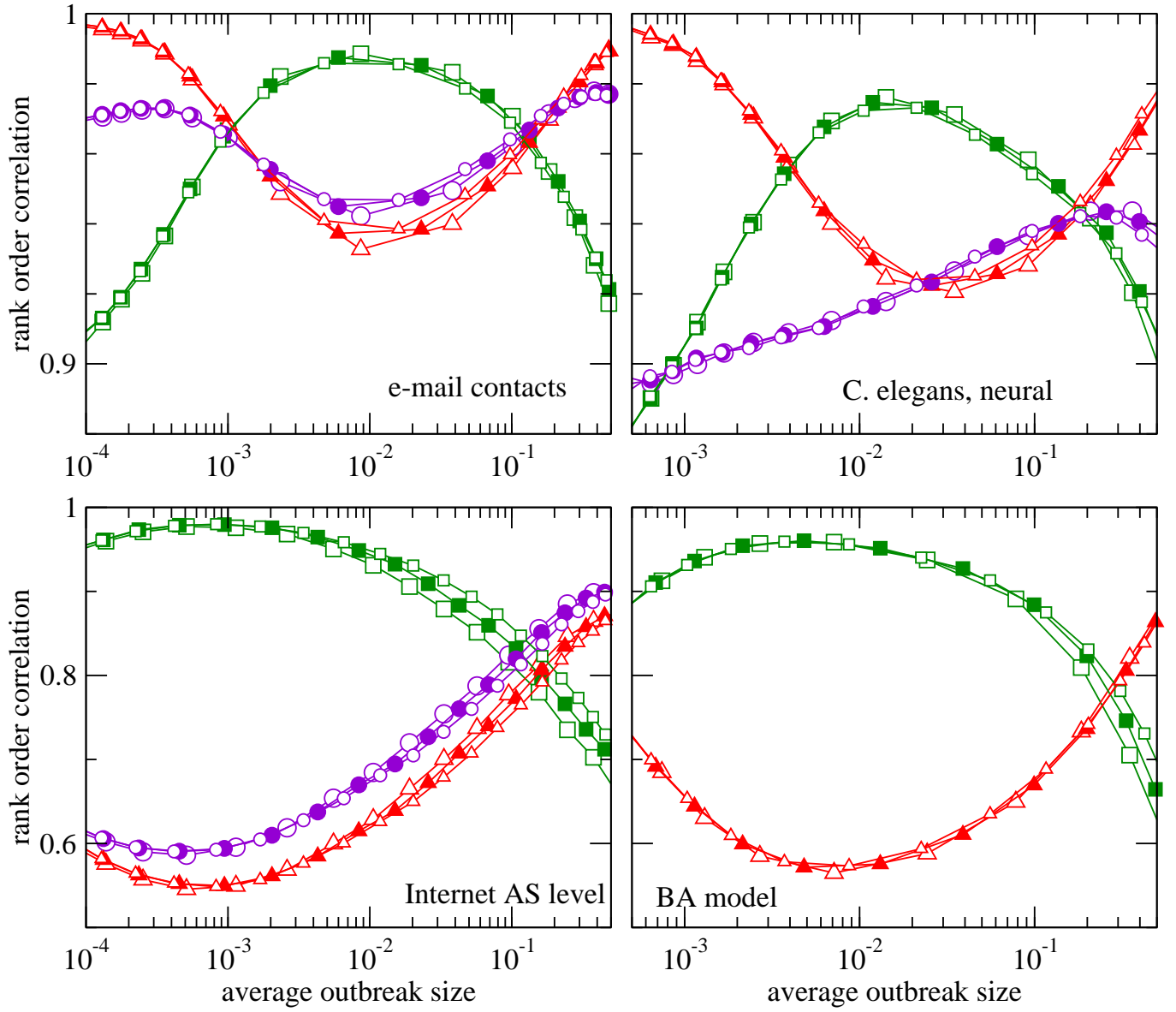


FIG. S2: Predictive power of different centrality measures for SIR spreading efficiency under varying recovery probability μ , distinguishing by small open symbols ($\mu = 0.1$), closed symbols ($\mu = 0.5$) and large open symbols ($\mu = 1.0$). Predictors are dynamical influence (squares), degree (triangles) and shell index (circles). The x-axis is the average outbreak size when seed nodes are chosen with equal probability. Further details are as in Figure 2 in the main article.

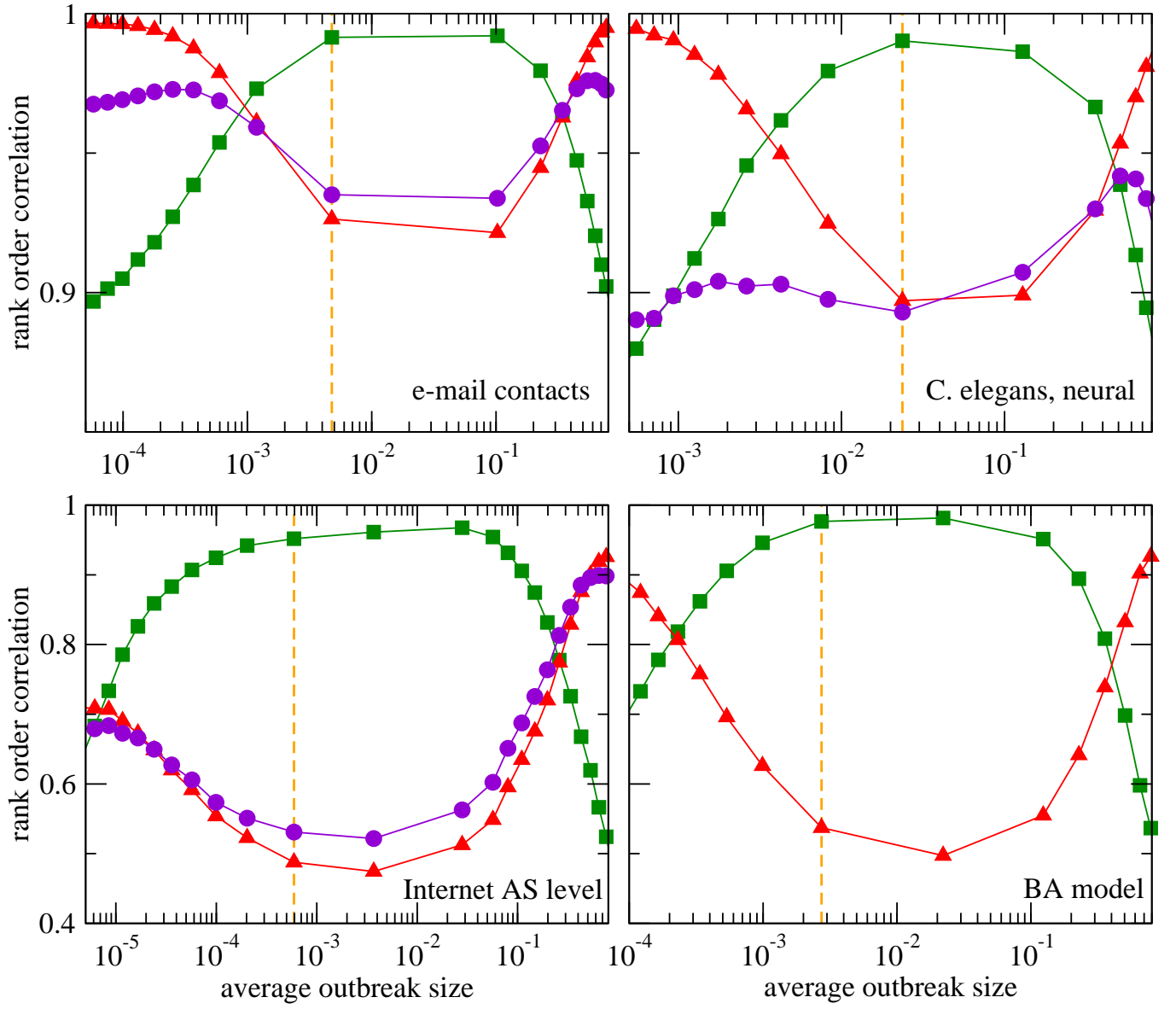


FIG. S3: Predictive power of different centrality measures for SIS spreading efficiency. Symbols are values of the rank order correlation coefficient of spreading efficiency with influence (squares), degree (triangles) and shell index (circles). Further details are as in Figure 2 in the main article.

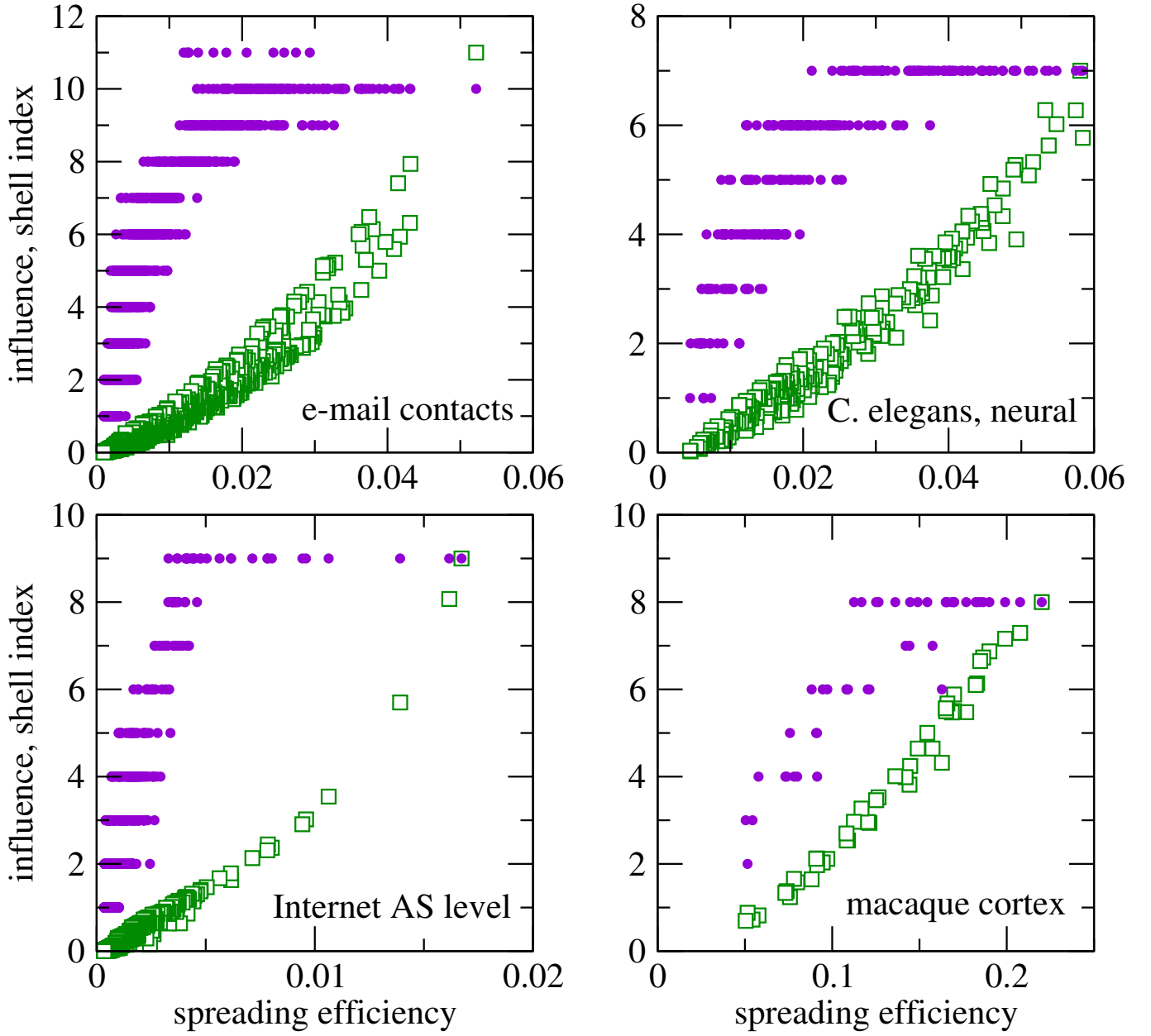


FIG. S4: Scatter plots of the shell index (filled circles) and influence (open squares) versus spreading efficiency in the critical regime. Each data point corresponds to a single node i in the given network with the abscissa giving the average outbreak size when seeding the SIR model at i . Parameter values are $\beta = 0.06$ (e-mail contacts), $\beta = 0.07$ (C. elegans), $\beta = 0.04$ (Internet), $\beta = 0.09$ (macaque cortex). In each of the four cases, the normalization of the influence vector c is chosen such that its maximum equals the maximum shell index k_{\max} .

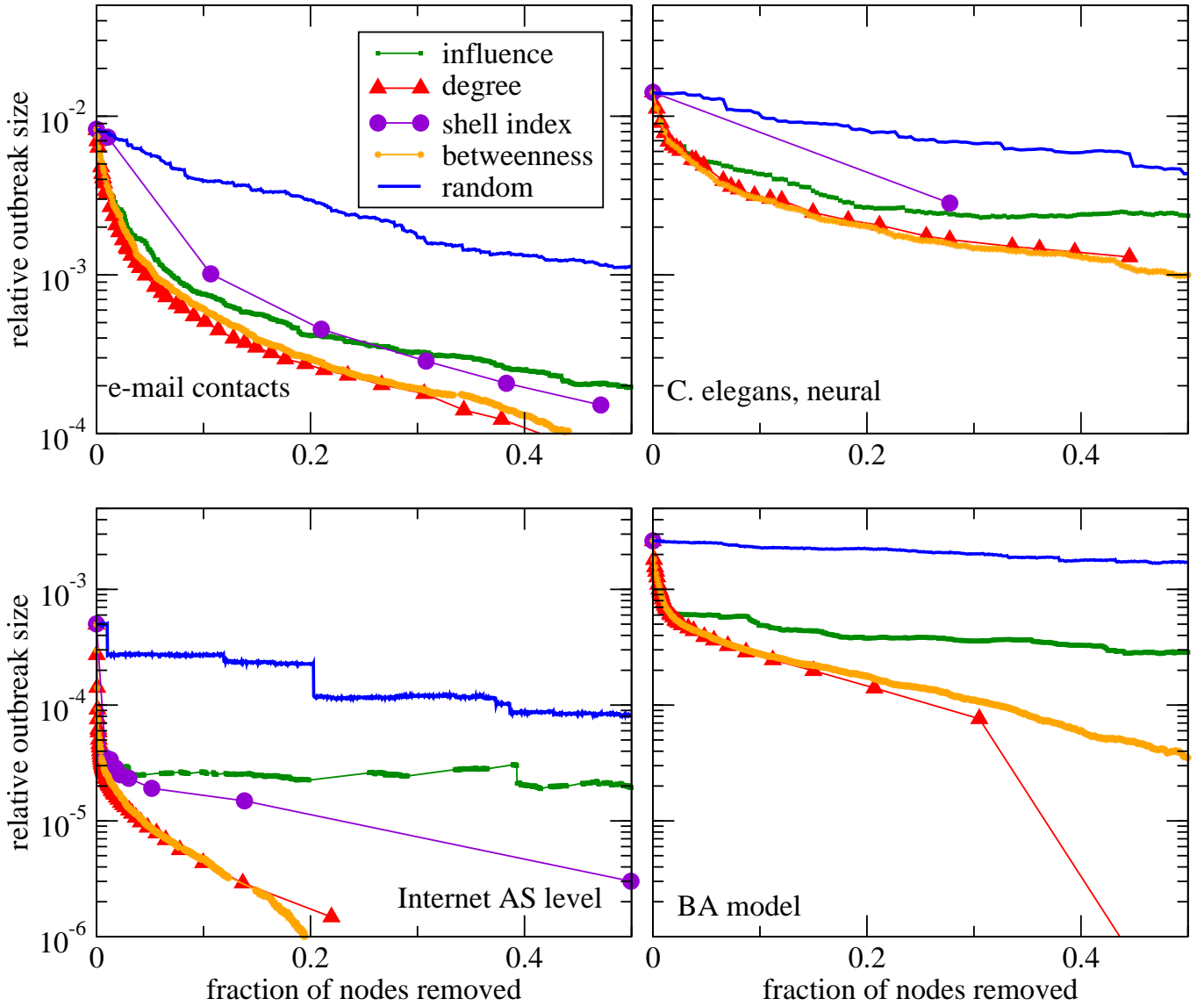


FIG. S5: Effect of node removal (vaccination) in the order of decreasing centrality on the average size of epidemic outbreaks in the SIR model at criticality. Partially vaccinated networks are obtained by removing the nodes with centrality value above a given threshold. Relative outbreak size is the average fraction of the remaining nodes reached by an infection. Each data point is an average over 10^6 realizations of the SIR process with seed nodes drawn uniformly and independently across realizations. In each network, the spreading parameter is chosen as $\beta = 1/\lambda_{\max}$, the inverse of the largest eigenvalue of the adjacency matrix. When β is two times or five times this value, qualitatively the same result is obtained. Note that centrality measures with discrete values (degree and shell index) produce fewer data points, because they assign the same value to larger sets of nodes.

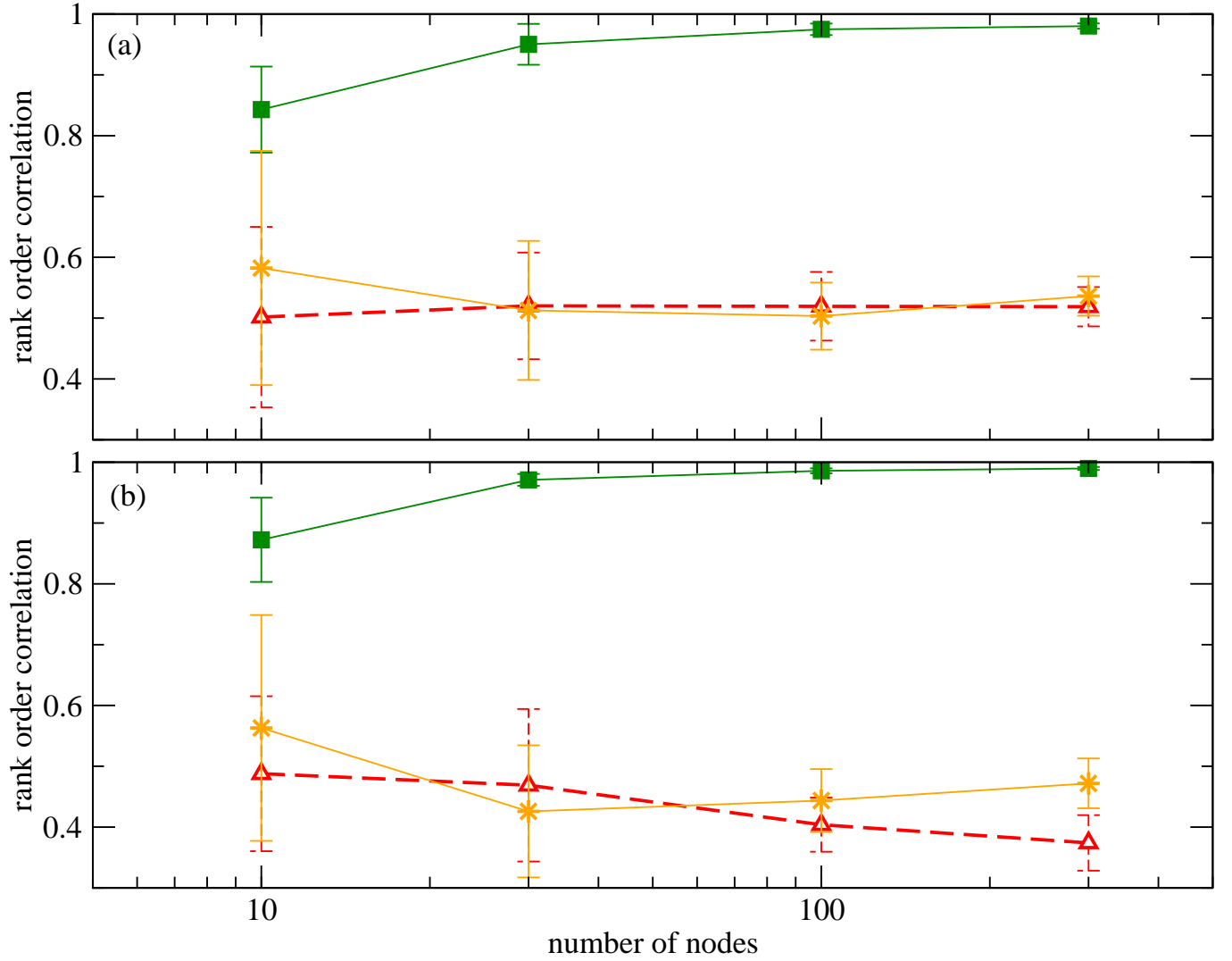


FIG. S6: Prediction of driving efficiency for Kuramoto oscillators on randomly grown directed networks of varying size. Each plotted point is the average rank order correlation between driving efficiency and Laplacian influence (squares), degree ratio (triangles), betweenness centrality (stars). Averages are taken over 10 independently grown networks. Error bars indicate the standard deviation. For panel (a), networks are initiated as two bidirectionally coupled nodes. Then at each step i of the growth process, a new node i attaches to the network with a link to a node j and another link from a node k , where j and k are chosen uniformly at random from the set of $i - 1$ existing nodes. For panel (b), the process of (a) is altered as follows. The choice of k is no longer uniform but node k is chosen with probability proportional to the out-degree of node k . This results in a scale-free out-degree distribution while keeping the in-degree distribution geometric. For the networks of panel (a), both in- and out-degree are distributed geometrically.

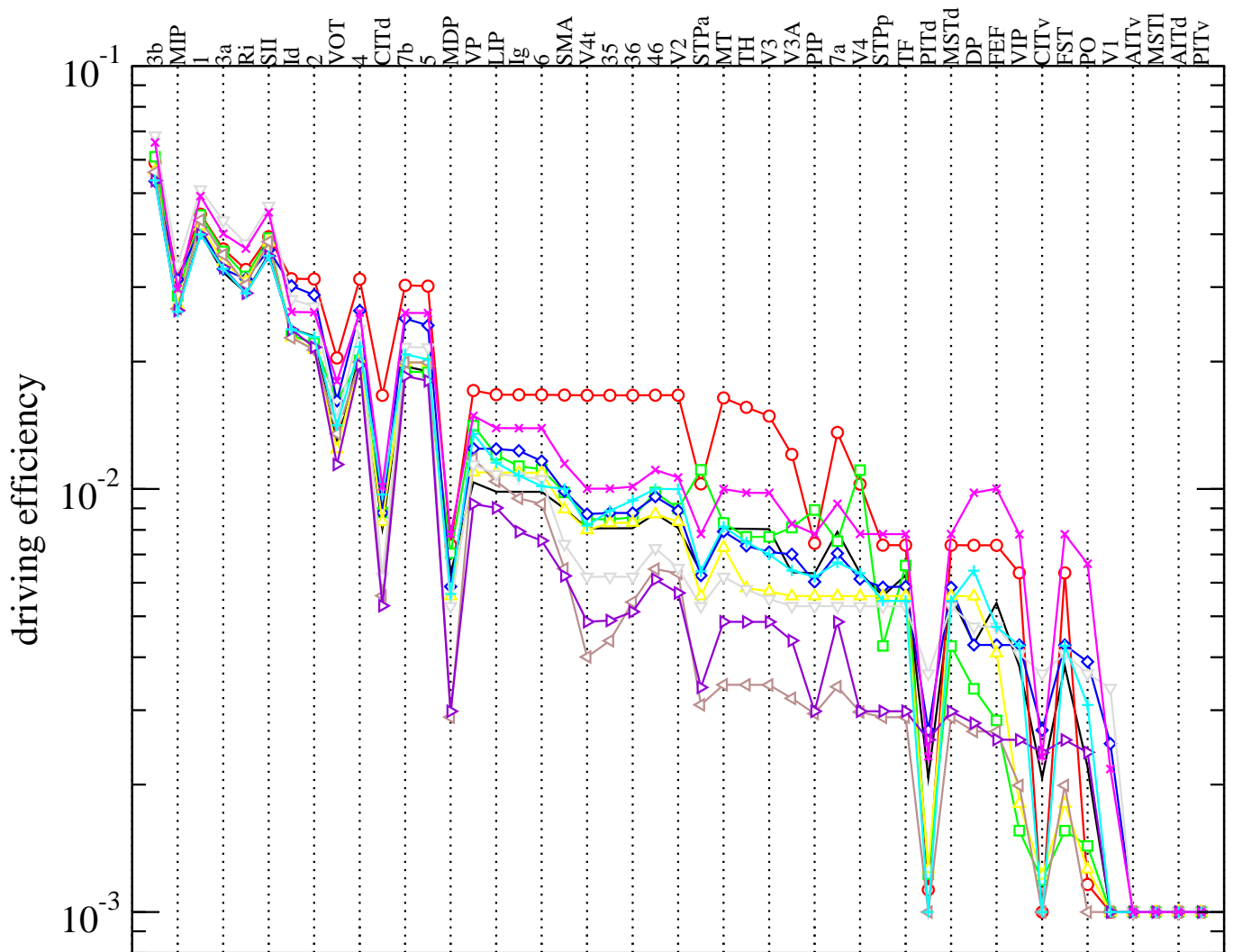


FIG. S7: Driving efficiency of nodes with Rössler oscillators on the Macaque cortex network. Nodes are ordered from left to right by decreasing dynamical influence. Symbols distinguish 10 independent random choices of initial conditions of the nodes in the network and the driving node.